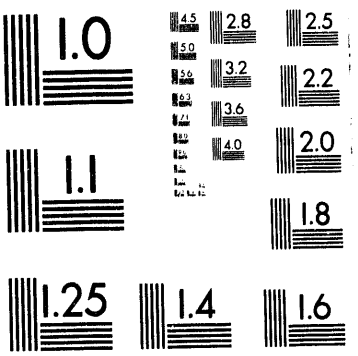
1.0
1.1
1.25
1.4
1.6
1.8
2.0
2.2
2.5
2.8
3.2
3.6
4.0
4.5
5.0
5.6

1 of 1

Conf-9211211--5

UCRL-JC-116851
PREPRINT

Spectroscopic Measurements of Rosseland Mean Opacity

P.T. Springer, D.F. Fields, B.G. Wilson, J.K. Nash, W.H. Goldstein, C.A. Iglesias, F.J. Rogers, J.K. Swenson, M.H. Chen, A. Bar-Shalom, and R.E. Stewart

This paper was prepared for submittal to the
Radiative Properties of Hot Dense Matter Workshop
Santa Barbara, CA
November 2-6, 1992

November 1992

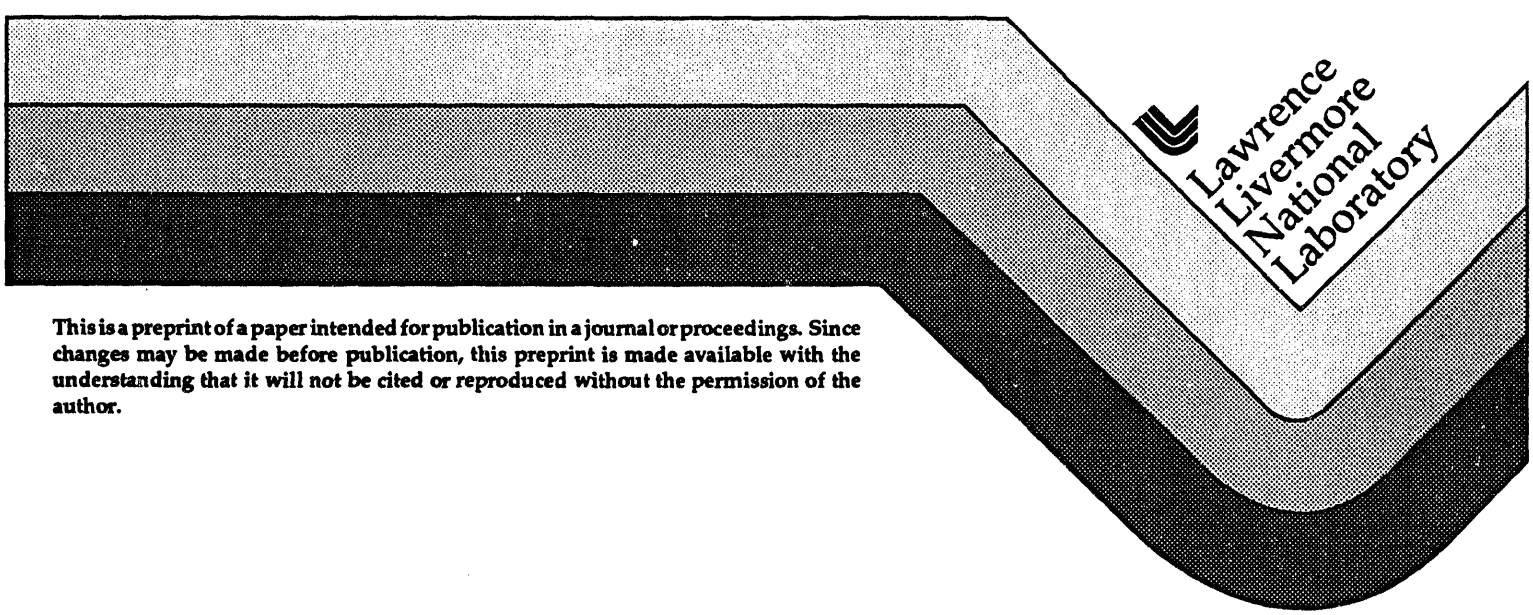

DISCLAIMER

Spectroscopic Measurements of Rosseland Mean Opacity

P.T. Springer, D.F. Fields, B.G. Wilson, J.K. Nash, W.H. Goldstein, C.A. Iglesias, F.J. Rogers, J.K. Swenson, M.H. Chen, A. Bar-Shalom, and R.E. Stewart

Lawrence Livermore National Laboratory, Livermore, California 94550

The first quantitative measurement of photoabsorption in the region determining Rosseland and Planck mean opacity, is obtained for an x-ray heated iron plasma, using novel techniques and instrumentation. The plasma density of 0.0113 +/- 0.0013 g/cc and temperature of 59 +/- 3 eV are accurately constrained experimentally by imaging plasma expansion and observing and modeling absorption in sodium dopant ions. The measured iron absorption spectrum is compared with several newly developed opacity models. The data constrains Rosseland and Planck group means with of order 15 percent precision. This is the first quantitative experimental certification of opacity models germane to radiative transfer in LTE plasmas.

The radiative properties of hot, dense matter are crucial to understanding systems ranging from stellar interiors to inertial confinement fusion plasmas[1]. Models for photo-absorption are complex, requiring knowledge of atomic structure, of level populations, of spectral line shapes, and of plasma interactions. The models often make simplifying assumptions and approximations owing to the enormous amount of atomic data required, and to the intractable nature of the many-body problem. In view of their complexity, their widespread utility, and their compromises, it is crucial to validate opacity models through well-characterized laboratory measurements.

Previous high precision photo-absorption measurements probed regions accessible to crystal spectroscopy[2-6]. While these measurements benefited opacity models, they did not access the spectral region lying near the peak of the Planck distribution, which dominates the radiative energy flow. Recent XUV measurements[7,8] have shown the gross character of photoabsorption in this band. In these studies, multiple shots on different targets were used to determine plasma absorption, and complex hydrodynamic simulations were used as a guide to temperature and density. Since opacity models depend critically upon plasma conditions, benchmark experiments require complete and precise characterization as well as precise transmission data. We describe new instrumentation and techniques that have allowed us to extend high-precision photo-absorption measurements into these soft x-ray and XUV spectral regimes. In the present work, the sample is spatially imaged to maximize the

precision of the transmission measurement, while simultaneous measurements accurately constrain the plasma conditions. All relevant experimental information is obtained in a single laser shot with a single target. These techniques have lead to the first highly constraining measurements of Planck and Rosseland mean opacities[9].

Accurate spectroscopic measurements of Rosseland mean opacity require an significant departure from traditional photoabsorption measurements using the technique of point-projection spectroscopy with time integrating instrumentation. This technique has been successfully used to obtain absorption spectra in the high energy crystal regime[2-5] , and has also been employed to accurately measure plasma density and temperature using low-z dopant ions simultaneous with the transmission measurement[2,3]. Unfortunately, this technique is restricted only to the highest energy portion of the spectrum where the plasma emission is weakest. The plasma emission backgrounds are accentuated since the emission is integrated over both time and space.

We depart from the method of point projection spectroscopy, and instead use grating spectrometers, time-gated detectors, pinhole imaging, and large area backlights. These new techniques allow measurements of the specific brightness of the sample and backlight emitters. In addition, the emission backgrounds are reduced and quantified, permitting accurate XUV measurements on higher temperature plasma. A factor of 20 reduction in emission backgrounds was obtained by using gated

microchannel plate detectors instead of film. Even so, this reduction in background only allowed the point projection technique to be extended down to the kilovolt range for the 50 to 100 eV plasmas described. The use of spatial imaging and areal backlighting further enhanced signal to noise, allowing the extension of absorption measurements into the sub kilovolt and XUV regimes, using either crystal or grating spectrometers. Using these techniques, we have measured the widths of transition arrays of mid-z plasmas in the sub kilovolt x-ray regime, and found that these widths depart from the predictions of the JJ coupled theories that succeed for high-z plasmas[10], but agree with the predictions of LS coupled models. We have also measured photoabsorption in the XUV regime where Rosseland and Planck mean opacities are determined, and have found reasonable agreement for certain classes of opacity models. This experiment is described below.

The NOVA laser at Lawrence Livermore National Laboratory is used to indirectly heat a tamped thin foil sample consisting of 132 $\mu g\ cm^{-2}$ of iron mixed with 55 $\mu g\ cm^{-2}$ of sodium fluoride. The 1000 x 300 μm foil is sandwiched between two larger 100 $\mu g\ cm^{-2}$ layers of Lexan, that act as a tamper and maintain a uniform spatial density in the heated sample. The 16 kJ, 353 nm heating laser has a duration of 1 ns and creates x-rays that radiatively heat the sample and cause it to expand.

The experimental setup is illustrated in Fig. 1. The tamped target is viewed edge-on by an XUV spectrometer through 300 μm of the foil, and is illuminated by a uniform 1 mm^2 area x-ray

backlight, created when a NOVA beam, smoothed by a random phase plate, strikes a gold foil. The sample is viewed edge-on in order to maximize the sample optical depth viewed from the spectrometer, while using a thin sample to insure uniform heating and small temperature gradients. A large optical depth is desired for accurate measurements in regions where the plasma transmission is high, since these regions strongly influence the Rosseland mean opacity. X-rays from the backlighting plasma are spatially imaged with 20 μm resolution, spectrally dispersed using a Hitachi 1200 lp mm^{-1} varied line spaced grating, and recorded on a two-dimensional image plane using a gated microchannel plate detector. The microchannel plate detector, with a CsI photo cathode, is active for 100 ps at 2 ns after the heating pulse begins. The spectrometer field of view is limited to 800 μm by a beryllium aperture between the plasma and spectrometer. The spectrometer magnification is 47, and the resolving power is of order 300. The spectral coverage of the spectrometer is from 50 to 325 eV, but the signal below about 80 eV is almost entirely due to higher order diffraction.

Figure 2 shows the image of the expanding plasma with a fully overlapped area backlight. The film optical density was measured versus position using a micro-densitometer. A film calibration wedge was applied to convert from optical density to x-ray exposure. The energy calibration was then performed using the positions of observed sodium, carbon, and beryllium absorption lines. The strength of the higher order diffraction images was obtained from the observed higher order absorption

features of beryllium and carbon. Images representing the second and third diffraction orders are normalized and subtracted from the data. Slight corrections for the second and third order diffraction for spectral regions above the Carbon Heα were obtained from another data set with higher spectrometer energy coverage.

Emission and background contributions were determined from a fit based on the depths of optically thick beryllium, carbon, and sodium transitions. The spectral shape of the background, and the absence of strong line emission features were confirmed in an auxiliary shot where the sample was viewed face-on with a backlight overlapping half of the sample. The image of the sample that had not been backlighted gives the emission backgrounds. With the background subtracted, the resulting image is of backlight x-rays that either pass through or to the sides of the sample, and are recorded in separate locations on the MCP detector. The plasma transmission is obtained by comparing the direct and attenuated x-ray signals.

The plasma density is determined from the measured width of the plasma and the known initial thickness of the foil. Iron and sodium are not uniformly mixed so that their absorption features are separately analyzed to give the individual mass distributions. The average density in the sample center is 0.0113 $\pm$ 0.001 g cm^{-3}, with a composition of 80.2 percent by weight iron. With the density fixed, the sodium absorption spectrum is then used to constrain the sample temperature. The technique employing the spectrum of light ionized elements has proven successful as a

plasma temperature diagnostic[2,3]. The sodium transmission spectrum shown in figure 3 is measured at the left edge of the sample (see Fig. 2) where the sodium and fluorine absorption features are strongest. The density at the sample edge is 0.00836 ± 0.0008 g cm^{-3}, with a composition of 91.1 percent by weight NaF. The sample mass density at the edge is lower than in the center due to the greater concentration of NaF. However, the free electron densities are comparable as required for pressure equilibrium. In Fig. 3 the iron absorption features are removed using the spectrum from the sample center where the iron features are strongest but normalized to the edge iron concentration. Typical uncertainties in the transmission data are indicated in Fig. 3. Fits to the sodium data determined the ratios of the optically thin lithium- and beryllium-like sodium lines. For these conditions, the strength of the beryllium-like lines are reduced relative to the lithium-like lines as temperature is increased and the sodium ionizes further. The same effect occurs with decreasing density, so an accurate density measurement is needed to determine the temperature.

The sodium spectrum was modeled using the OPAL opacity code[11] coupled to spectroscopically accurate atomic data generated by a multiconfiguration Dirac-Hartree-Fock code (MCDF) using intermediate coupling[12]. The calculations include states from ionization sequences Helium-like through Boron-like and levels with principal quantum number up to n=7. The ionization balance in OPAL is based on a systematic expansion of the grand canonical partition function[13]. Figure 3 shows the sodium

several photon energy points. The results of two STA calculations using the measured density of 0.0113 g cm^{-3} and sample temperatures of 57 and 59 eV are shown in Fig. 4a which illustrates the sensitivity of the models to temperature.. The results for the MCUTA and OPAL/DTA models at the measured density and 59 eV temperature are compared to the data in Figs. 4b and 4c, respectively. Note that the model spectra have not been smoothed to account for experimental resolving power.

OPAL was also used with two different approximations in the atomic physics. The first employs the detailed configuration accounting (DCA) which neglects term splitting. The second uses the same DCA method, but with the term splitting included with the unresolved transition array (UTA) approximation assuming LS coupling[17]. Figure 4d shows the OPAL model with UTA method, and Fig. 4e shows the OPAL model with the DCA approximation. An OPAL/DCA calculation where the computed oscillator strengths are replaced by hydrogenic values is not shown, but resembles the OPAL/DCA results in Fig. 4e. All of the opacity models that include term broadening match the observed spectrum fairly well, although there are discrepancies in absorption coefficient as large as 60 percent in the spectral regions with high transmission. The OPAL/DCA calculation, which neglects term splitting, is in poor agreement with the data, and the absorption coefficient can have as much as a factor of 10 error.

The transmission spectrum is converted to a frequency dependent photoabsorption coefficient by taking the logarithm and dividing by the areal density of 339 $\mu g\ cm^{-2}$. The absorption

coefficient was integrated with the Planck and Rosseland weighting functions in the spectral region of 100 to 300 eV. The resulting group mean opacities are given in Table 1. Note that at this temperature this spectral interval encompasses the most important energy region of the weighting functions. The error estimates in the group mean opacities are due to uncertainties in the subtraction of higher order diffraction and emission backgrounds. The experimental value of Planck mean may be underestimated if sharp absorption features are not adequately resolved. The size of this error was estimated using smoothed model spectra to simulate experiment. Using the STA model, the experimental Planck mean is underestimated by 3 percent, and using the OPAL/DTA model, the corresponding error is 14 percent. Group mean opacities were computed for the models in the same spectral region as the data and the results tabulated in Table 1. While there is not a large variation in Planck and Rosseland mean values predicted by the models for these conditions, the precision of the data is sufficient to distinguish the importance of term broadening in computing the Rosseland mean opacity. For this plasma, jj coupled models without configuration interaction perform as well as *LS* models. This finding is contrary to the results for inner-shell transitions in iron[10].

Using new techniques and instrumentation, we have accurately measured the frequency dependent absorption of a well-characterized, radiatively heated iron plasma, resulting in estimates of Rosseland and Planck group mean opacities accurate to 15 percent. The plasma density is determined from the spatial

extent of the expanded plasma and the plasma temperature is inferred from the ionization distribution of sodium ions doped in the plasma. With plasma conditions constrained by measurements, several different opacity models are compared with the measured iron spectrum. This measurement constitutes the first quantitative experimental certification of opacity codes in the spectral region germane to radiative transfer in LTE astrophysical and laboratory plasmas.

We would like to thank C. Bruns and J. Emig for helping assemble the experiment, J. Ticehurst for her help with the analysis, R. Wallace for his assistance in target preparation, and the NOVA crew for operating the laser. This work was performed under the auspices of the U.S. Department of Energy by the Lawrence Livermore National Laboratory under Contract No. W-7405-ENG-48.

1. Radiative Properties of Hot Dense Matter, eds. W. Goldstein, C. Hooper, J. Gautier, J. Seely, and R. Lee (World Scientific, Singapore, 1991)

2. T. S. Perry *et al.*, Phys. Rev. Lett. **67**, 3784 (1991)

3. P.T. Springer *et al.*, *Atomic Processes in Plasmas*, eds. E.S. Maramar and J.L. Terry, (AIP, New York, 1991), pp. 78

4. J. M. Foster *et al.*, Phys Rev Lett. **67**, 3255 (1991)

5. S.J. Davidson *et al.*, Appl. Phys. Lett. **52**, 847 (1988)

6. J. Bruneau et al. Phys. Rev. **A44**, 832(1991); and references therein

7. L. Da Silva *et al.*, Phys. Rev. Lett. **69**, 438 (1992)

TABLE 1. Planck and Rosseland group mean opacities in $cm^2 g^{-1}$

	Planck	Rosseland
Experiment	8200 ± 700	4400 ± 600
STA	8431	4630
MCUTA	8226	4525
OPAL/DTA	8188	4100
OPAL /UTA	8257	4255
OPAL /DCA	8169	2997
Hydrogenic DCA	10974	2723

8. W. Schwanda and K. Eidmann, Phys. Rev. Lett. **69**, 3507 (1992)

9. P.T. Springer et al., Phys Rev. Lett. 69, 3735 (1992)

10. P.T. Springer *et al.*, in preparation

11. F.J. Rogers and C.A. Iglesias, Ap. J. Supplement, **79**,507 (1992)

12. I.P. Grant *et al.*, Comp. Phys. Commun. **21**,207 (1980); B. J. McKenzie *et al.*, Comp. Phys. Commun. **21**, 233 (1980);M.H. Chen, Phys. Rev. **A31**, 1449 (1985)

13. F.J. Rogers *et al.*, Ap. J. **310**, 723 (1986) and references therein.

14. A. Bar-Shalom *et al.*, Phys. Rev. **A40**, 3183 (1989); A. Bar-Shalom *et al, Atomic Processes in Plasmas,* eds. E.S. Maramar and J.L. Terry, (AIP, New York, 1991), pp. 68

15. B. G. Wilson *et al., Atomic Processes in Plasmas,* eds. E.S. Maramar and J.L. Terry, (AIP, New York, 1991), pp. 189

16. F.J. Rogers, B.G. Wilson, and C.A. Iglesias, Phys. Rev. **A38**, 5007 (1988)

17. C. Bauche-Arnault, J. Bauche, and M. Klapish, Adv. At. Mol. Phys. **23**, 131 (1988)

DATE
FILMED
4/11/94
END